Synthesis of Crystalline, Nanometer-Scale, −(CH$_2$)$_x$− Clusters and Films on Gold Surfaces

Kannan Seshadri,[†] **Sundar V. Atre,**[‡] **Yu-Tai Tao,***[,§] **Mong-Tung Lee,**[§] **and David L. Allara***[,†,‡]

Contribution from the Departments of Chemistry and Materials Science and Engineering, Pennsylvania State University, University Park, Pennsylvania 16802, and Institute of Chemistry, Academia Sinica, Taipei, Taiwan 115, Republic of China

Received December 23, 1996[⊗]

Abstract: Stable, nanometer-scale thickness films of −(CH$_2$)$_x$− have been observed to form by the surface-catalyzed decomposition of CH$_2$N$_2$ on evaporated Au film substrates. In the early stages, growth occurs in the form of isolated clusters at defect regions in the {111} textured surfaces. As the average thickness increases beyond ∼20 nm, growth spills out onto the {111} terraces with eventual coverage of the entire surface. At all coverages, the dominant structure is highly *trans*, extended polymethylene chains packed in an orthorhombic lattice, similar to the typical structure of crystalline, bulk-phase polyethylene but containing more conformational defects than well-formed bulk crystals. Chain melting occurs at ∼135 °C, and cooling to room temperature results in differing extents of ordering as a function of the total film coverage, an indication that the structures of the growing films are constrained in metastable forms by the presence of adjacent gold surface defect features. The polymerization mechanism appears to involve surface-catalyzed decomposition of the diazomethane at gold defect sites to produce methylidene adsorbate species, which subsequently initiate the formation of linear polymers via a free radical propagation process. This process provides a useful limiting case of the surface-catalyzed formation of linear hydrocarbons from C$_1$ intermediates on transition metals.

1. Introduction

The preparation of highly structured, low-defect, ultrathin polymer coatings is of considerable interest for both scientific and technological applications. Scientifically, there is much current interest in the effects of dimensionality and substrate interaction on the fundamental properties of polymer films as thicknesses approach the correlation lengths of single polymer chains,[1] and on a more applied level, for example, chemists have long been interested in the modification of electrode surfaces with ultrathin films for controlled electrochemistry.[2] Technologically, there is high interest in the fabrication of stable, ultrathin, high-performance films for applications in areas such as microelectronics and packaging. Polyolefins, which are highly inert, exhibit favorable properties for protective films and have found diverse applications in the areas of coatings. The simplest member of the family, linear polyethylene with the elementary −(CH$_2$)− repeat unit, is also the most difficult of the common polyolefins to process. While the surface and bulk properties of highly linear −(CH$_2$)$_x$− materials are well understood, little is known about the properties of ultrathin films of nanometer-scale thicknesses, since no way has yet been developed to make such films in a simple, reproducible manner, primarily because of the relative insolubility which precludes the use of standard solution casting methods. There have been reports of using plasma polymerization to attach polyethylene films to gold surfaces,[3] but these surfaces were previously modified by adsorption of a monolayer of organosulfur com-

pounds, the film compositions were reported to be nonstoichiometric, and the incorporation of significant amounts of oxygen was observed.

While the direct polymerization of ethylene on surfaces is limited to extremely specific catalyst materials such as Ziegler−Natta catalysts employing supported TiCl$_3$, there have been indications that one possible route to the formation of high-quality, ultrathin polymethylene (PM; or alternatively, polyethylidene) films could involve a surface-catalyzed decomposition of CH$_2$X species, particularly diazomethane (CH$_2$N$_2$; DM):

$$x\text{CH}_2\text{N}_2 \xrightarrow{\text{surface catalyzed}} -(\text{CH}_2)_x-(\text{surface}) + \text{N}_2(\text{gas}) \quad (1)$$
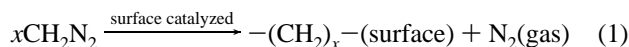
One of the earliest references to the polymerization of aliphatic diazo compounds is that of Bamberger and Tirchner,[4] who observed that ethereal solutions of diazomethane on long storage contain a white precipitate of the composition (CH$_2$)$_x$. Shortly after, Loose[5] and Lorey[6] determined that powdered copper metal and its salts catalyze the decomposition of aliphatic diazo compounds such as diazoacetic ester and ω-diazotoluene to produce olefins. Since that time, a number of workers have noted the formation of polymeric material from both homogenous and heterogeneous catalytic decomposition of aliphatic diazo compounds, but in the case of the surface-catalyzed decompositions the character of the surface coatings has never been clearly established. Buckley *et al.*[7] investigated the decomposition of a series of diazoalkanes ranging from DM to higher primary compounds, e.g., diazobutane, and observed that polymerization occurred in the presence of copper powder as well as with copper salts, BF$_3$, triphenyl borate, and tricyclo-

---

† Department of Chemistry, Pennsylvania State University.
‡ Department of Materials Science and Engineering.
§ Institute of Chemistry, Academia Sinica.
⊗ Abstract published in *Advance ACS Abstracts,* May 1, 1997.
(1) Calvert, P. M. *Nature,* **1996,** *384,* 311.
(2) Bard, A. J.; Abruña, H. D.; Chidsey, C. E. D.; Faulkner, L. R.; Feldberg, S. W.; Itaya, K.; Majda, M.; Melroy, O.; Murray, R. W.; Porter, M. D.; Soriaga, M. P.; White, H. S. *J. Phys. Chem.,* **1993,** *93,* 7147−7173.
(3) Stewart, K. R.; Whitesides, G. M.; Godfried, H. P.; Silvera, I. F. *Rev. Sci. Instrum.* **1986,** *57,* 1381−3.

---

(4) Bamberger, E.; Tirchner, F. *Ber. Dtsch. Chem. Ges.* **1900,** *33,* 956.
(5) Loose, A. *J. Prakt. Chem.* **1909,** *79,* 507.
(6) Lorey, H. *J. Prakt. Chem.* **1930,** *124,* 185.
(7) Buckley, G. D.; Cross, L. H.; Ray, N. H. *J. Chem. Soc.* **1950,** *1950,* 2714−2718.

hexylborate.[8] These workers also found that mixtures of DM with higher diazoalkanes such as diazododecane react under similar conditions to produce side chain polymers and that high molecular weight PM ($\sim 3 \times 10^6$) results from a BF_3 catalyst.[9] A study of the polymerization kinetics with copper stearate and BF_3 catalysts showed the rate to be first order in monomer and catalyst concentrations but the molecular weight to be independent of the concentrations.[10] Physical properties such as crystallinity, melting points, and molecular weight have been reported for bulk samples of both homo- and copolymers formed from various diazoalkanes.[11] Both radical (carbene-like) and ionic mechanisms have been proposed.[12,13] While these studies serve to make the case that a variety of bulk-phase polyolefins can be produced by a number of different catalytic methods, little information was reported with regard to the nature of surface processes. However, a few reports have cursorily dealt with this aspect. It has been reported that $AuCl_3$- and $AuBr_3$-catalyzed PM formation from DM[14] involves intermediate formation of catalytically active gold colloids.[15,16] Treatment by hot xylene was reported to remove a PM residue of MW $\sim 10^4-10^5$ to leave ~ 1.3 nm diameter gold colloids.[17] In addition, recovery of a bulk sample of a related polymer, polyethylidene [$-(CHCH_3)_x-$], has been reported after decomposition of diazoethane in the presence of metals.[17] Neither the structures of the metal surfaces nor the surface-bound polymer films were directly studied, but it was observed that different metals have different catalytic activities. From these indirect observations a generalized reaction mechanism was proposed whereby the polymerization proceeds through carbene (ethylidene)-type intermediates coordinated to active sites on the metal surfaces,[17,18] although the issue of the growth mechanism after complete coverage of the metal substrate was not addressed. In a study of polymerization on an iron surface, it was suspected that polyethylidene forms via intermediates similar to those involved in the Fischer-Tropsch synthesis.[19,20] There have been peripheral reports of PM formation from DM decomposition on a variety of surfaces including those on silicone grease,[21] bentonite interlayers,[22] and SiO_2,[23] but the origin of the catalytic activity remains unclear. We emphasize the point that in spite of this significant body of work there is a lack of understanding of the actual surface-bound structures and formation mechanisms of even the simplest hydrocarbon polymers, e.g., PM, which form directly on characterized surfaces via diazoalkane decomposition.

Drawing upon the above precedent for metal surfaces to catalyze the formation of polyalkylidenes via diazoalkane decomposition, we initiated studies of the growth of polymethylene films on freshly evaporated gold surfaces. Through the application of surface characterization techniques—in particular, ellipsometry, infrared spectroscopy (IRS), high energy ion forward recoil elastic scattering (FRES), atomic force microscopy (AFM), quartz crystal microgravimetry (QCM) and liquid drop contact angles—we have observed that crystalline PM films are readily formed in the thickness range of 1−100 nm. The films initially nucleate as nanometer-scale clusters at defect sites in the Au surface but cross over to a continuous surface coverage with increasing DM decomposition. These results show a new way for preparing nanometer-scale polyolefin films and clusters with well-organized structures and bring a useful parallel to the understanding of the formation of hydrocarbon polymers during transition metal surface catalyzed reactions of hydrocarbons.

2. Experimental Section

1. Materials. Diazald (*N*-methyl-*N*-nitroso-*p*-toluenesulfonamide, obtained from Aldrich Chemical, St. Paul, MN) was used for the preparation of diazomethane. Ether (anhydrous; Aldrich Chemical, St. Paul, MN) was used as received. Hexadecane (99.99%; Aldrich Chemical, St. Paul, MN) was dehydrated by agitating a $\sim$1:1 mixture with sulfuric acid in a standard separatory funnel. The mixture was allowed to stand for 30 min after which the hexadecane was decanted off and immediately passed through a column of activated alumina (Aldrich grade II). Organic-free, deionized water of high resistivity ($>$18.0 MΩ cm) was obtained by use of a Millipore Purification System (Bedford, MA). The base substrates in all experiments except AFM were either polished Si(100) wafers or optical quality fused silica disks (ESCO, Inc., Plainfield, NJ). For AFM freshly cleaved mica substrates (green mica, ASTM V-2 quality, Asheville-Schoonmaker Mica Co., Newport News, VA) were used.

2. Sample Preparation. Diazomethane was prepared as an ethereal solution from Diazald according to literature procedures.[24] The yellow stock solution decomposed slowly with time, and this made it necessary to titrate it with benzoic acid solution to determine the concentration. The stock solutions were diluted to different concentrations with ether just before use. All solutions were prepared in polypropylene containers which were thoroughly cleaned before use with multiple rinses of water and ethanol followed by drying in a stream of N_2. Gold substrates for all experiments except some AFM runs were prepared by an initial deposition of $\sim$10 nm of Cr followed by $\sim$200 nm of gold (99.999%) onto either clean silicon wafers or 1/16 in. thick quartz disks. All depositions were carried out at pressures $<3 \times 10^{-7}$ Torr. These films exhibit rms surface roughnesses of $\sim$1.0−1.5 nm and previous studies have established that our preparation methods produce a polycrystalline morphology with a high {111} surface texture.[25] Immediately after deposition, ellipsometry measurements were made on the set of samples, which required $<$3 min per sample, and then the gold films were transferred directly into the DM solutions, pre-cooled to 0 °C. In any given set of multiple samples, the total exposure to the ambient atmosphere for the last one was limited to 15 min. The substrates were taken out of solution at the end of the immersion period, washed with pure ether and then absolute ethanol, and finally dried by spinning. The immersion times and concentrations were varied according to the nature of the study. The substrates for some of the AFM samples studied were made by evaporation of $\sim$120 nm of Au directly onto freshly cleaved mica heated at 340 °C at $<3 \times 10^{-7}$ Torr. Further heating *in vacuo* for 1 h was carried out to anneal the samples to give typical grain sizes of $\sim$300 nm as observed by AFM.[26] PM films were made on these substrates as described above.

(8) Buckley, G. D.; Ray, N. H. *J. Chem. Soc.* **1952**, *1952*, 3701−3704.

(9) Kantor, S. W.; Osthoff, R. C. *J. Am. Chem. Soc.* **1953**, *75*, 931−932.

(10) Feltzin, J.; Restaino, A. J.; Mesrobian, R. B. *J. Am. Chem. Soc.* **1955**, *77*, 206−210.

(11) Richardson, M. J.; Flory, P. J.; Jackson, J. B. *Polymer* **1962**, *4*, 221−235.

(12) Dorion, G. H.; Polchlopek, S. E.; Sheers, E. H. *Angew. Chem.* **1964**, *76*, 495−496.

(13) Mucha, M.; Wunderlich, B. *J. Polym. Sci.* **1974**, *12*, 1993−2018.

(14) Saini, G.; Campi, E.; Parodi, S. *Gazz. Chim. Ital.* **1957**, *81*, 342−353.

(15) Saini, G., Nasini, A. G. *Atti R. Accad. Sci. Torino* **1955**−**56**, *90*, 586.

(16) Ledwith, A. *Chem. Ind.* **1956**, 1310.

(17) Nasini, A. G.; Trossarelli, L.; Saini, G. *Die Makromol. Chem.* **1961**, *44*−*46*, 550−569.

(18) Nasini, A. G.; Trossarelli, L. *J. Polym. Sci.* **1964**, *C4*, 167−171.

(19) Muetterties, E. L.; Stein, J. *Chem. Rev.* **1979**, *79*, 479−490.

(20) Loggenberg, P. M.; Carlton, L.; Copperthwaite, R. G.; Hutchings, G. J. *Surf. Sci.* **1987**, *184*, L339-L344.

(21) Kubota, H.; Morawetz, H. *J. Polym. Sci., Part A-1* **1967**, *5*, 585−591.

(22) Bart, J. C.; Cariati, F.; Erre, L.; Gessa, C.; Micera, G.; Piu, P. *Clays Clay Miner.* **1979**, *27*, 429−432.

(23) Tsusumi, K.; Hagiwara, S.; Takahashi, H. *Nippon Kagaku Kaishi* **1973**, 1374−1378.

(24) de Boer, T. J.; Backer, H. J. *Organic Syntheses*; Wiley: New York, 1963; Collect. Vol. IV, pp 250−253.

(25) Nuzzo, R. G.; Fusco, F. A.; Allara, D. L. *J. Am. Chem. Soc.* **1987**, *109*, 2358−2368.

(26) Chidsey, C. E. D.; Loiacono, D. N.; Sleator, T.; Nakahara, S. *Surf. Sci.* **1988**, *200*, 45−66.

3. Characterization

1. Ellipsometry. Ellipsometry measurements were done at a single wavelength of 632.8 nm with a Rudolph AutoEL-II Null Ellipsometer (Rudolph Instruments, Fairfield, NJ) at 70° angle of incidence. The polarization parameters Δ and Ψ (related to the polarizer and analyzer) were recorded at several arbitrarily chosen spots on the sample. Readings were taken on the freshly deposited gold substrates to obtain the bare substrate optical constants. Measurements were then performed on the polymethylene/Au samples after the film deposition and the film thickness determined from the two sets of ellipsometric responses. The instrumental precision was 0.04°, and the overall sample-to-sample error resulting from this is ∼0.1 nm.

2. Contact Angle. Measurements were made with a Rame-Hart Model 100 contact angle goniometer. Deionized water and hexadecane were used as the wetting liquids. The sample surfaces were in an atmosphere containing the saturated vapor of the wetting liquid. The chamber was maintained at 20.0 ± 0.5 °C. Static, sessile drops were delivered from a flat-tipped micropipet. Contact angle hysteresis was also measured by using a horizontal stage with the volume of the test liquid held between the tip and sample changed to keep the area of the surface−liquid contact constant.

3. Infrared External Reflection Spectroscopy. General details of the technique are reported elsewhere.[27] The spectra are recorded in absorption units of reflectivity, $-\log(R/R_o)$, where R_o is the reflectivity of a reference gold film sample which was cleaned of surface contaminants in a UV-ozone chamber (AAI-ABTECH, Model UVC-100, Yardley, PA) prior to use. Annealing experiments were performed *in situ* with a modified sample holder that contacted the sample back to a heated copper slab. Fused quartz disks ($^1/_8$ in. thick) were used for these experiments, and the sample temperature was measured by insertion of a chromel−alumel thermocouple junction in a drilled hole running radially into the sample edge. The chamber was continuously purged with dry nitrogen, and temperature control was provided by a temperature controller (Omega Instruments, Stamford, CT).

4. Atomic Force Microscopy (AFM). Imaging of the films was performed with a Digital Instruments Nanoscope III AFM (Digital Instruments, Santa Barbara, CA) with 1.1 and 14 μm range piezoelectric scanners. The scans were performed in air both in the tapping mode and in the contact mode to explore image quality. All images were fit to a plane with use of the instrument software and were also filtered to remove noise. Line scans were performed to investigate the cluster dimensions.

5. Forward Recoil Elastic Scattering (FRES). FRES measurements were done on the samples at the Tandetron ion accelerator facility at Cornell University with use of a 2.77-MeV He^{2+} beam. The sample was bombarded until the net charge delivered reached a preset value. The recoiling H atoms were with using a MCP detector and the detector geometry allowed an energy resolution of ∼53 keV. A mylar stopper foil was used to absorb any He^{2+} ions that recoil in the forward direction. The film thickness was obtained by simulating the experimentally obtained spectrum with the knowledge of the surface composition and stoichiometry. Simulations were performed with use of the RUMP software package (obtained from the Cornell University Ion Accelerator Facility.)

6. Quartz Crystal Microgravimetry (QCM). The PM growth was investigated by using highly polished quartz crystals with vacuum-deposited gold electrodes (AT cut, 5 MHz resonant frequency, Maxtek Inc., Torrance, CA) driven by a home-built oscillator with ±0.1 Hz frequency error. Two types of runs were made. In a batch type run, the gold electrode surfaces were first cleaned with UV-ozone and then the oscillation frequency was measured "dry", *viz*, with the sample in air. Following that, the sample surface was again cleaned and then immediately immersed in the DM solution. After reaction, the sample was removed and washed (see above) and then reconnected to the oscillator circuit for a dry measurement. In the *in situ* mode, the cleaned crystal was connected to the oscillator circuit and then immersed in the DM solution. The frequency shift was monitored in real time during the film formation process with use of gating times of several seconds for the frequency counting.

(27) Parikh, A. N.; Allara, D. L. *J. Chem. Phys.* **1992**, *96*, 927−945.
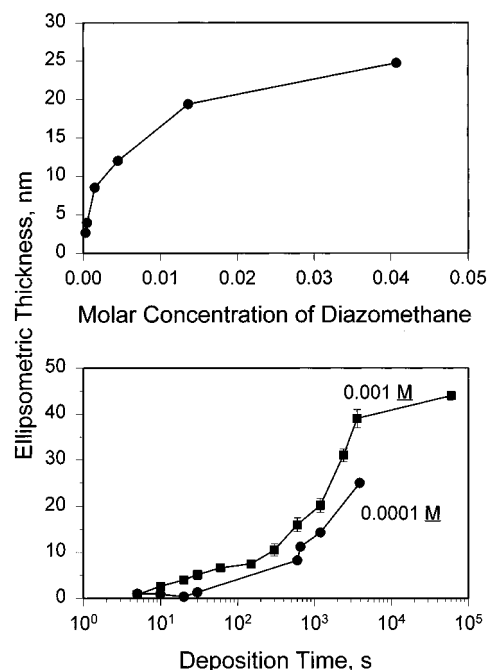

Figure 1. Top: PM film thickness as a function of DM concentration in ether solution for constant 3.0 min immersion times at 0 °C. Bottom: Dependence of PM film thickness on deposition time for 0.0001 and 0.001 M DM solutions. Thicknesses were estimated from ellipsometry measurements by using the full-density, uniform film approximation (see text).

4. Results

1. Optical Ellipsometry. Since changes in the ellipsometric response of the gold surfaces provided a quick measure of the amount of polymer deposited on the gold surfaces, this technique was used to survey the effects of DM concentration and the immersion time. Figure 1 shows plots of film thickness vs DM concentration, for a constant immersion time of 3 min, and increasing deposition time for two DM concentrations. The thicknesses were determined with use of classical electromagnetic theory[28] formulated for a parallel-layer model consisting of an air/film/substrate structure. The film was approximated as a uniform isotropic slab with a refractive index of 1.50, a value within the range reported for polyethylene.[29] We show later that this assumption of a uniform structure is incorrect for the thinner films, and more accurate film thickness values will be determined based on the structural models developed from other data such as AFM. However, for purposes of a qualitative characterization of growth conditions, the data in Figure 1 are quite informative and can be used as a measure of the average total coverage of the film. One point to note in the figures is that the film growth rates level off with increasing concentration and time, an indication that the polymerization rate slows with increasing thickness. Also, film thicknesses obtained by multiple immersions are roughly the same as those from a single immersion with equivalent total length of time. Ellipsometric response was also used as an indicator of stability. The PM films were found to be extremely resistant to conventional solvents, and the average coverages were unaffected by prolonged storage in ambient laboratory conditions, for times even up to a year. However, significant film loss was observed

(28) Azzam, R. M. A.; Bashara, N. M. *Ellipsometry and Polarized Light*; North-Holland: Amsterdam, The Netherlands, 1977.

(29) Typical polyethylene refractive index values in the optical region are 1.49 and 1.52 for amorphous and crystalline materials [see: *Polymer Handbook*, 2nd ed.; Immergut, E. H., Brandrup, J., Eds.; J. Wiley and Sons: New York, 1975; with further reference to: Bryant, W. M. D. *J. Polym. Sci.* **1947** 2, 556].
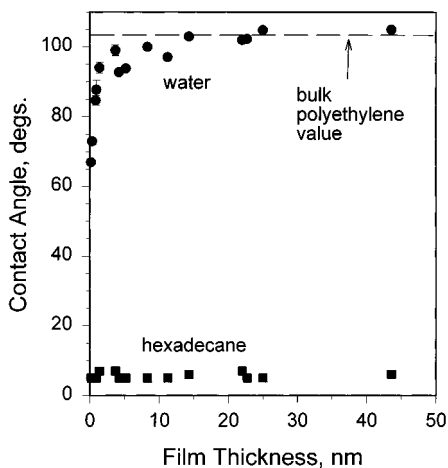
Figure 2. Water and hexadecane advancing contact angles as functions of the PM film thickness. Thicknesses were estimated from ellipsometry measurements by using the full-density, uniform film approximation (see text).

upon exposure to hot toluene and xylene, notably good solvent conditions for polyethylene.

2. Wetting Behavior. It was observed in all cases that hexadecane wets the film surface. This behavior is consistent with the well-known oleophilic character of polyethylene. However, the contact angle for water depends strongly on the substrate roughness and the total film coverage.

For the smooth Au films, deposited at high vacuum on smooth substrates, a clear correlation exists between water contact angle and film growth, as shown in Figure 2. These data indicate that the overall film structure changes considerably with growth; films with ∼20 nm thickness show the contact angle of ∼103° expected for pure polyethylene surfaces, but with decreasing thickness the angles drop to a low value of ∼85°. In addition, we observe a substantial contact angle hysteresis of ∼30° for films of thickness up to ∼6.0 nm with a drop to ∼20° at thicknesses above ∼25.0 nm. A large hysteresis can be taken as an indication of a heterogeneous surface that is capable of extensive pinning of the water drop at high energy localities.[30] These data thus suggest that the surfaces of the thinner films are quite heterogeneous with bare gold regions which become covered as the films grow. For a bare gold surface exposed to ambient conditions where typical associated adventitious organic contaminants are adsorbed, we observe water contact angles of ∼65−67°. On this basis the wetting behavior can be modeled by using the approximate relation:[31]

$$\cos(\theta) = \sum [f_i \cos(\theta_i)] \qquad (2)$$

where θ and θ_i are the equilibrium contact angles of the composite surface and the pure surface of the ith component, respectively, and f_i is the *effective* mole fraction of the ith component in the wetting surface layer. Using eq 2 with the contact angle values of 103 and 65° for the pure PM and ambient Au surfaces, respectively, leads to PM coverages of ∼8−10, 48−55, and 85−100% for films of thickness of the order of 1.0−5.0, ∼25.0, and ∼40.0 nm, respectively. These numbers

(30) A recent study on model heterogeneous surfaces consisting of alternating hydrophilic and hydrophobic strips reveals that these systems are characterized by a contortion of the three-phase contact line for liquid drops present on the surface. The advancing and receding contact angles were lower by 2−10° when measured with the strips normal to the contact line than those measured with the strips tangential to the three-phase line. See, Drelich, J.; Wilbur, J. L.; Miller, J. D.; Whitesides, G. M. *Langmuir* **1996**, *12*, 1913−22.

(31) Cassie, A. B. D. *Discuss. Faraday Soc.* **1948**, *3*, 11−16.

provide a very useful qualitative picture of the evolution of structure with film growth.

3. Atomic Force Microscopy. In order to confirm the discontinuous nature of the low-coverage films surmised from the wetting data, PM films grown on Au films supported on mica substrates were scanned by AFM with the cantilever in the tapping mode. Figure 3a shows the topography of a bare gold/mica surface which contains large {111} terraces with sizes near 400 nm. Figure 3b shows an image of a PM film with a coverage that has been estimated from ellipsometry to be equivalent to a uniform planar film ∼1.7 nm thick. The image clearly shows the expected grain boundaries of the gold, but in some locations there are accretions of material with spheroidal to elongated shapes which are not present on the bare gold surface. These features appear primarily in the grain boundary regions of the gold, and we attribute them to PM clusters. These clusters also appear at other gold imperfections such as pinholes. For example, Figure 3c shows an image taken on the same sample at sites that tend to disrupt the large terrace, and similar features are seen. Figure 3d shows a 3-D rendering of the clusters in frame 3c to show their vertical profile. The larger peak heights are ∼6 nm. Imaging was also conducted on films grown on Au/quartz substrates. In contrast to the bare gold structure on mica, the gold deposited on quartz has smaller {111} terrace regions and exhibits a rolling hills and valleys type of morphology, as seen in Figures 3e and 3f for a PM film with a coverage approximately equivalent to a 5.5 nm, uniform, planar film. The features are not unlike those grown on mica substrates. The film growth again appears to originate from grain boundaries. As the average coverage increases, we observe (data not shown) that these features become more smeared, indicating that the clusters grow laterally outward. The films grown on the mica-supported gold typically exhibit clusters of vertical dimensions between 2 and 60 nm with lateral dimensions of several tens of a nanometer. We caution that these dimensions should be considered in a qualitative way since distortions may result from different tip-sample interactions as well as instrument drift. In contrast to the ease of obtaining dimensional information as well as clear images on the Au/mica, the more undulating topography of the Au/Cr/SiO₂ substrates makes it difficult to assign reliable dimensions to the clusters on these substrates, but there is no *a priori* reason to expect any significant differences from those formed on the Au/mica ones.

4. Infrared Spectroscopy. The IRS measurements were made in order to elucidate the molecular structure and chain packing of the PM clusters. Survey spectra, covering both the low- and high-frequency regions, are given in Figure 4A for the cases of PM films with equivalent coverages (from ellipsometry) of 1.0, 4.0, and 44.0 nm. All the spectra exhibit similar qualitative features expected for extended −(CH₂)ₓ− chains: CH₂ rocking, CH₂ bending (scissors deformation), and C−H stretching bands at ∼725, 1470, and 2850−2950 cm⁻¹, respectively. However, the intensities for the C−H stretching modes do not show a linear correlation with the measured ellipsometric thickness. This can be the result of the inadequacy of ellipsometry in describing the thickness and/or the formation different structures (e.g., chain orientation) with increasing thickness. As will be discussed later in thermal behavior, it is believed that the latter is of importance.

a. High Frequency Region. Figure 4B shows in detail the overlaid C−H stretching mode spectra for an ultrathin (1.0 nm) and a thick (44.0 nm) film. For the thicker film, the symmetric (d⁺) and antisymmetric (d⁻) stretches for the CH₂ unit appear as strong bands peaked at 2851 and 2920 cm⁻¹, respectively. In addition, a shoulder appears at ∼2895 cm⁻¹. This shoulder

(a) 1.25 μm
(b) 1.25 μm

(c) 250 nm
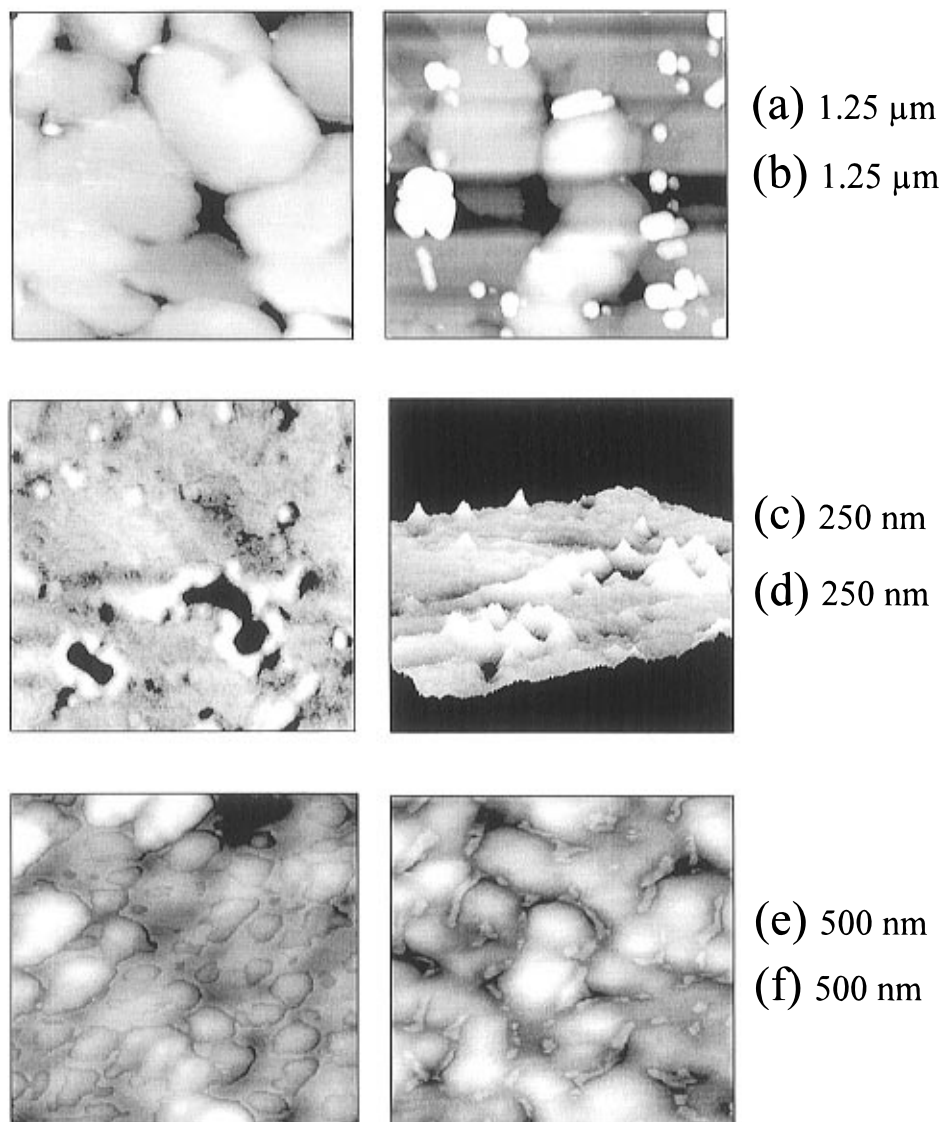**(d)** 250 nm

(e) 500 nm
(f) 500 nm

Figure 3. Tapping mode AFM surface images taken with a 1.1-μm scanner. Film thicknesses were estimated from ellipsometry measurements by using the full-density, uniform film approximation (see text). In the gray scale used, black and white represent the lowest and highest points, respectively. (a, top left) Bare gold substrate formed by vacuum deposition of 120 nm of gold on mica. Note the relatively flat grains produced by the annealing process carried out immediately after deposition. (b, top right) A 1.7 nm thick PM film on a gold/mica substrate made in the same way as the one in image a. The height of the brightest regions corresponds roughly to 30 nm. The parallel horizontal lines are artifacts of the tapping mode line scan. (c, middle left) The same sample as in part b but focusing on a region in a (111) terrace. The PM films are seen to grow as clusters from defect regions in the terrace. (d, middle right) The same image as in part c but rendered in three dimensions to show the vertical projection of the clusters. The tops of the highest clusters are approximately 6 nm. (e, lower left) A 200-nm gold film vacuum deposited on a quartz disk primed with a 10-nm layer of chromium. The average grain size is ~120 nm, a smaller value than observed on the Au/mica films (image a), and there are relatively few flat regions on the surface. (f, lower right) A 5.5-nm PM film deposited on the same substrate as in image e. The films appear in the form of isolated clusters situated in the regions between crystalline grains.

is typically observed in polyethylene spectra, but its origin is unclear.[32] Values of 2849 and 2917−2918 cm^{-1} have been reported for the d$^+$ and d$^-$ mode peak frequencies, respectively, for single crystals of polyethylene,[33] while corresponding values for alkyl chains typically range from 2846−2850 and 2915−2920 cm^{-1}, respectively, for extended, high *trans* conformations.[34] In contrast, conformationally disordered chains typically show values of ~2856 and ~2928 cm^{-1}, again respectively.[35] In comparison, the observed d$^+$ and d$^-$ frequencies of 2851

and 2920 cm^{-1} for the PM/Au film lie at the upper edge of values reported for conformationally ordered polymethylene chain assemblies. These data indicate that the film chains, while conformationally ordered, must contain some degree of *gauche* defects.[33] Such defects could arise from an occasional chain kink (e.g., *tgt* or *gtg'* defect) and/or from the presence of some degree of organized chain folding to produce lamellae, typical for polyethylene crystals. The broad structure of the clusters depicted in the AFM images suggests that the PM chains may contain occasional single gauche kinks (*tgt*) since domains of low-*gauche* defect, all-*trans* chains should appear as long rod-like structures while the presence of gauche kinks would disrupt this linear structure. As the PM film thickness decreases from 44.0 to 1.0 nm, the defect content rises to some extent as seen

(32) Previous work has assigned this band to either the b_{3u} component of the antisymmetric CH stretch or a combination of the Raman and infrared active CH$_2$ bending modes. [See ref 24 and the following earlier report: Nielsen, J. R.; Holland, R. F. *J. Mol. Spectrosc.* **1961**, *6*, 394.]

(33) Painter, P. C.; Runt, J.; Coleman, M. M.; Harrison, I. R. *J. Polym. Sci. Polym. Phys. Ed.* **1977**, *15*, 1647−1654.

(34) Snyder, R. G.; Schaachtschneider, J. H. *Spectrochim. Acta* **1963**, *19*, 85−116.

(35) Snyder, R. G.; Strauss, H. L.; Elliger, C. A. *J. Phys. Chem.* **1982**, *86*, 5145−5150.
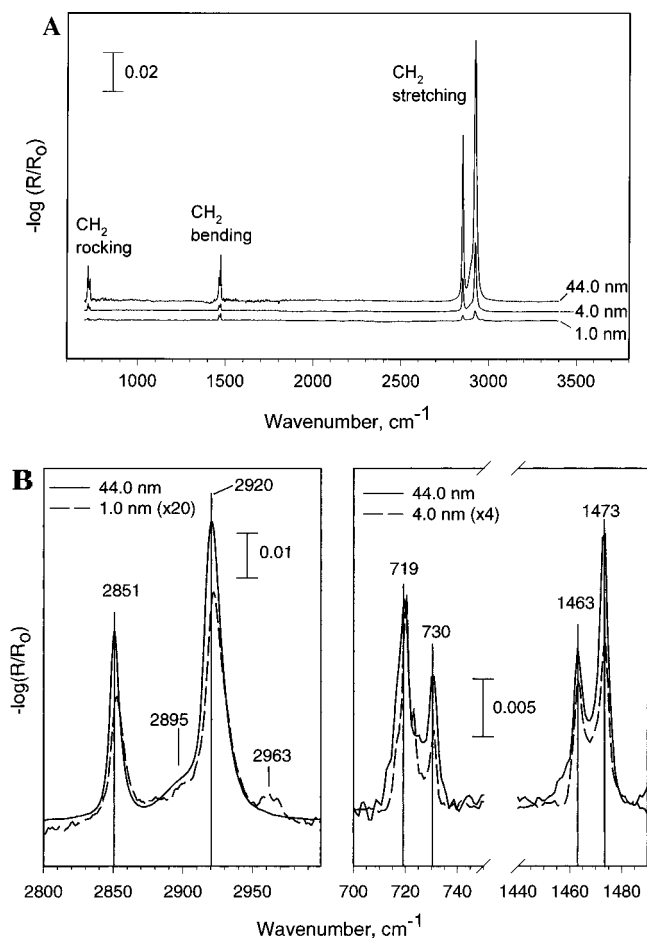
Figure 4. (A) Panoramic Infrared spectra showing the major absorption features for 1.0, 4.0, and 44.0 nm thick PM films. Film thicknesses were estimated from ellipsometry measurements by using the full-density, uniform film approximation (see text). (B) Expanded spectra showing the details for the three major absorption features shown in part A. For the C−H stretching mode region spectra are shown for the 1.0 and 44.0 nm thick films, and the former spectral intensity is multiplied by 20 in order to show details on the selected intensity scale. In the low-frequency region the 1.0 nm film spectrum is replaced by the 4.0 nm one since the signal to noise of the former is too weak to show details in the rocking region; the intensity is scaled by a factor of 4. Note the appearance of the CH_3 asymmetric stretch at ∼2963 cm^{-1} in the 1 nm film spectrum. Given the scale factor of 20, if the same identical feature were present in the 44.0 nm film spectrum its presence would be largely masked by the extremely intense d$^-$ mode tail.

in Figure 4 by the ∼1−3 cm^{-1} increases in the d$^+$ and d$^-$ frequencies and the similar increase in the line widths. This observation shows that the initial nucleation stage of the PM clusters involves considerable chain disorder, intermediate between the crystalline and liquid states. One can also note in the 1.0 nm film spectrum the presence of a weak band at 2963 cm^{-1}, which is assigned to the asymmetric CH_3 C−H stretching mode (r$^-$). Since the observation of this weak signal is very reproducible and does not change with extensive solvent rinsing, the presence of the CH_3 group can be considered as an intrinsic structural feature in the ultrathin PM films. This observation suggests that polymer chain propagation occurs via radical intermediates with the termination involving radical disproportionation:

$$RCH_2CH_2^{\bullet} + R'CH_2CH_2^{\bullet} \rightarrow RCH_2CH_3 + R'CH=CH_2 \quad (3)$$
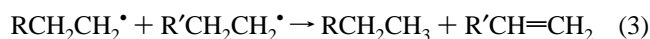
where R and R′ represent two different chain radicals which

are adjacent. This reaction implies the presence of the −CH=CH₂ group but, within the signal to noise ratio obtainable, no peaks were observed in the characteristic frequency regions for the vinyl group.[36]

b. Low Frequency Region. Overlaid rocking and scissors deformation mode spectra are given in Figure 4B for 4.0- and 44.0-nm films. The 1.0-nm film, used as the example of an ultrathin film in the C−H stretching region spectra (see above), was replaced by the 4.0-nm film since the intensities of the rocking mode features did not appear above the noise in the 1.0-nm case. The doublet splitting of the CH_2 scissoring deformation mode, with features at 1463 and 1473 cm^{-1}, indicates that the chains are packed in a crystalline lattice with the presence of two chain configurations per unit subcell, a characteristic of an orthorhombic chain packing.[37,38] The narrow peak widths, characterized by the full widths at half maximum (fwhm) of 5−8 cm^{-1}, indicate that the associated crystalline structure is well-developed with large correlation lengths.[39] In agreement with this structure, the rocking band is also split into a doublet with components at 720 and 730 cm^{-1}. While it is well-established[40] that these two components can arise from out-of-phase and in-phase deformations, respectively, between adjacent chains in an orthorhombic subcell, with the splitting determined by the chain spacings,[37,40] it also is known that the presence of other polymer morphologies can give rise to peaks in this region.[41] For example, the presence of monoclinic and amorphous phases each can give rise to a single peak at ∼718 and 720 cm^{-1}, respectively.[42] In a pure orthorhombic phase, the intensity ratio for the peaks at 730 and 720 cm^{-1}, I_{730}/I_{720}, has been theoretically determined to be 1.233, and this value has been verified experimentally for the cases of crystalline *n*-alkanes and polyethylene.[43] Applying this relationship, the full set of spectra show that films in the 20-44 nm thickness range have an orthorhombic crystalline lattice content of ∼60−65%. This content decreases to as low as ∼15−20% for films in the 4 nm thickness range, but we caution that the spectra become too noisy in the ultrathin film region to make reliable estimates. On the presumption that the only crystalline habit present is the orthorhombic one, then one can assign the remaining 720 cm^{-1} peak intensity phase to the presence of conformationally disordered chains. These chains could be

(36) The presence of the vinyl peak at 1640 cm^{-1} (for C=C stretch mode) as well as 909 cm^{-1} (for out-of-plane bending mode) can be seen readily for films thicker than 60 nm. These peaks were present along with a weak peak at ∼1368−1373 cm^{-1} (attributed to the symmetric methyl bending modes. Snyder, R. G. *J. Mol. Spectrosc.* **1961**, *7*, 116−144).

(37) Snyder, R. G. *J. Mol. Spectrosc.* **1961**, *7*, 116−44.

(38) Hagemann, H.; Strauss, H. L.; Snyder, R. G. *Macromolecules* **1987**, *20*, 2810−9.

(39) Krimm, S.; Liang, C. Y.; Sutherland, G. B. B. M. *J. Chem. Phys.* **1956**, *25*, 549.

(40) Stein, R. S. *J. Chem. Phys.* **1955**, *23*, 734−6.

(41) Stein, R. S.; Sutherland *J. Chem. Phys.* **1953**, *21*, 370−371.

(42) There are three major crystalline packings for alkyl chains, orthorhombic, triclinic, and monoclinic, but only the orthorhombic can account for our observed doublet splitting. Paraffins that crystallize into a triclinic form (characterized by one chain per unit cell) have a single methylene rocking band at 717 cm^{-1} (Holland, R. F.; Nielsen, J. R. *J. Mol. Spectrosc.* **1962**, *8*, 383). In the monoclinic subcell, where the chains are aligned parallel to each other, correlation splitting is neglible with a singlet at 718 cm^{-1} accompanied by a singlet at 1475 cm^{-1} (ref 34 in this paper and: Painter, P. C.; Havens, J.; Hart, W. W.; Koenig, J. L. *J. Polym. Sci. Polym. Phys.* **1977**, *15*, 1237−49). However, it has been observed that distortion of an orthorhombic lattice by rotation of a small number of chains, which lead to a local monoclinic structure, can lead to vibrations near 717 cm^{-1}. The existence of the monoclinic form has been reported in the case of polymethylene under conditions of stress, such as shaken preparations of polymethylene crystals (Kikuchi, Y.; Krimm, S. *J. Macromol. Sci. Phys.* **1970**, *B(4)*, 461−72) and cold drawing of polyethylene (Schmidt, P. G. *J. Polym. Sci.* **1963**, *1A*, 1271).

(43) Zerbi, G.; Gallino, G.; Del Fanti, N.; Baini, L. *Polymer* **1989**, *30*, 2324−2327.

present in a completely amorphous phase and/or in lamellar folds associated with the surfaces of high molecular weight crystallites. This issue will be addressed again in the discussion of the thermal annealing results.

We note that none of the spectra show discernible features in the 740−1110-cm^{-1} region. In this region, crystalline *n*-alkanes typically exhibit a series of peaks arising from coupled rocking−twisting modes[34] which are associated with the ν_8 dispersion curves in the polymethylene chain.[44] However, in the case of long PM sequences, such as found in typical crystalline polyethylene samples,[38] the higher frequency band spacings decrease to the point that they no longer are resolved. The presence of only the lowest frequency members of these bands in our spectra supports the conclusion that the PM chains have grown, on average, to a considerable extent beyond that of typical alkane molecules. Another mode progression, the twist−wag modes, is found in alkanes in the 1150−1350-cm^{-1} region. As in the case of the rock−twist modes, the higher frequency twist−wag modes for long PM sequences are not resolved, and in general, for chain lengths beyond C_{20}, the individual bands merge to a continuum.[45] In addition, neither the spectra of high molecular weight polyethylene ($M_w = \sim 10^5$) in a highly drawn state with long extended *trans* sequences[46] nor low molecular weight polyethylene ($M_w = \sim 1800$)[38] reveal the presence of the progression bands. Thus we conclude that our PM sequences must at least exceed ~ 20 CH_2 units. This can be expected on the basis of early work by Nasini *et al.*,[17] who showed that PM of molecular weights as high as $\sim 10^5$ can be recovered from decomposition of DM on gold colloids.

Since a number of features in the spectra indicate that the average chain is in a largely all-trans conformational state, the chain can be considered as a rigid rod for which it is possible, in principle, to determine a chain tilt angle, relative to the substrate surface, from the spectral intensities by using classical electromagnetic theory in conjunction with the optical function frequency spectrum of the film material.[27] Such calculations were attempted, but the initial efforts were not successful because of difficulties in obtaining accurate optical function spectra and in accurately accounting for discontinuities in the films (clusters and voids).[47] An indication of the latter type of problems can be seen from the nonlinearity of the IRS peak intensities with thickness, exemplified in Figure 4B.

5. Higher Accuracy Film Thickness Calculations. Our initial treatment of the ellipsometric data assumed a parallel slab, air/film/substrate model. In this model, each layer was

(44) Snyder, R. G. *J. Chem. Phys.* **1979**, *71*, 3229−35.

(45) Snyder, R. G. *J. Chem. Soc., Faraday Trans.* **1992**, *88*, 1823−33.

(46) Glenz, W.; Peterlin, A. *J. Macromol. Sci. Phys.* **1970** *B4*, 473−90.

(47) Orientation calculations were attempted, but difficulties were encountered in two areas. First, it was difficult to obtain reliable optical functions of pure forms of polymethylene similar to that in our films. For example, one convenient reference state is provided by isotropic dispersions of monodisperse, low molecular weight polyethylene (MW $\sim$1000) in KBr matrices. However, the spectra of such material differed sufficiently from our films, e.g., the C−H stretching region, that derived optical functions were not considered reliable for our calculations. Another reference state considered was long-chain alkanes, e.g., $C_{44}H_{90}$, where the effect of the CH_3 groups is statistically neglible. However, these materials exhibit somewhat different band shapes for some important peaks, e.g., C−H stretching, than our PM films, and the optical functions were not considered as accurate models for our purposes. The second, and perhaps most important, difficulty arises from the complicated morphologies of the films. The thinner films consist of isolated clusters embedded to some extent within the depths of gold defect regions whereas the thicker films, while nominally continuous, most likely exhibit considerable void contents. Optical response simulations for these types of morphologies require the use of effective medium approximations. In the present case, the accuracy of the simulations will be subject to the inherent uncertainties in the film structures with respect to the composition of gold, air, and PM. Further rigorous studies of these chain orientation calculations are in progress and will be reported elsewhere.
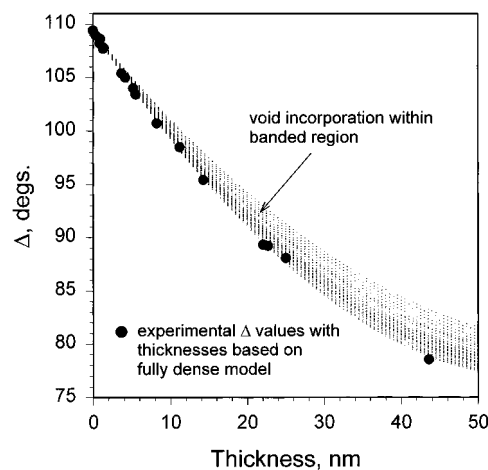
Figure 5. Calculated film thicknesses from the ellipsometric parameter data Δ. The calculations are based on a composite film model of isotropic PM clusters with void regions in between. The void fractions have been varied over a wide range of possible values, and optical constants were varied over the realistic range of values of 1.48−1.52 for a PM phase. The shaded region on the plot indicates the range of possible thicknesses for the variations in void content and optical functions. The filled circles represent thicknesses calculated for experimental Δ values by using a model incorporating no voids, *viz.*, a fully dense PM layer. For details see text.

considered as a uniform material of homogeneous composition, and the optical constants of the Au and PM layers were taken from the bare substrate responses and the independently known scalar value of $n_{iso} = 1.50 + 0i$ for polyethylene, respectively. While this assumed treatment is sufficient to generate estimates of the average film coverages, the AFM images, which reveal a strongly non-uniform density distribution to the growing films, show that the assumed parallel slab model must be modified in order to provide better interpretations of the ellipsometric data. Accordingly, the film was treated as a simple composite of regions of spheres of isotropic material interspersed in a void with a thickness defined by the average height of the tops of the PM spheres. The optical constants for each composition were calculated by using the Maxwell-Garnet approximation.[48] A range of PM refractive indices from 1.45 to 1.51 were considered, and void fractions were varied from 0.05 to 0.96. Figure 5 shows the calculated range of thicknesses for given values of Δ, the most sensitive ellipsometric parameter. For reference, the thicknesses which were calculated from experimental Δ values on the basis of the 100% dense PM layer model (no voids) are shown as filled circles. Based on the AFM images one can expect that the most realistic effective film thickness values for the clustered film structures, *viz.*, $\lesssim$40 nm, will come from the middle portion of the banded region in Figure 5 where the void contents are $\sim$50%. The plot shows accordingly that the film thicknesses based on the fully dense PM layer may be too low by as much as $\sim$10−15%.[49]

6. Quartz Crystal Microgravimetry. Determinations of the total masses of the PM films were made from QCM measurements with the Sauerbrey relation:[50]

(48) Maxwell-Garnet, J. C. *Philos. Trans. R. Soc.* **1904**, *203*, 885.

(49) In addition to incorporating the discontinuous character of the film in the ellipsometric model, a more rigorous treatment should consider the possibility that the chains may be uniformly aligned, likely parallel to the substrate, thus giving rise to film anisotropy. On this basis the film optical functions should be desribed in terms of second rank tensors. We have performed calculations based on an anisotropic PM-void composite model, which incorporates the known birefringence of alkyl chains, and find that the ellipsometric thicknesses are even lower by $\sim$10% than from the isotropic composite model.

(50) Sauerbrey, G. *Physik* **1959**, *155*, 206.

$$\Delta f = \frac{-2f_o^2 \Delta m}{A(\rho_q \mu_q)^{1/2}} \qquad (4)$$

where Δf is the crystal oscillation frequency shift for mass loading of Δm, f_o is the fundamental crystal oscillation frequency, nominally 5 MHz in our measurements, A is the electrode surface area, and μ_q and ρ_q are the crystal elastic shear modulus and the crystal density with the respective values of 2.947×10^{11} g cm^{-2} s and 2.648 g cm^{-3}. The film thicknesses were then calculated by assigning a density of 0.92 g cm^{-3} for PM. Figure 6 correlates the mass loading thicknesses for a typical series of films with the estimated ellipsometric thicknesses calculated on the simplest basis of a fully dense (no voids) PM layer approximation. The least-squares slope of the line is 1.34, indicating a consistently lower estimated thickness from ellipsometry. Since the QCM-derived thicknesses involve no inherent morphological models, the discrepancy can be associated primarily with the model-dependent ellipsometry values. However, as noted above, if the ellipsometric thicknesses are calculated by modeling the PM layers as air/polymer composites, the ellipsometric thicknesses will *increase* by ~10−15%, depending upon the actual void content. While this increase closes the gap between the two sets of thickness values, it does not bring them into agreement quantitatively. However, the comparison reinforces the picture of the film growth as occurring via cluster formation. We note that ellipsometry calculation models which incorporate chains aligned parallel to the surface can bring agreement between the QCM and ellipsometric thicknesses.[49]

7. Forward Recoil Elastic Scattering. In order to strengthen the quantitation of coverages, a series of deuterated PM (dPM) films were prepared from deuterated diazomethane, CD₂N₂ (dDM), and then analyzed for total counts of the H and/or D atoms per unit film area by FRES. The use of deuterated material eliminates interferences from adventitious H-containing impurities since D and H are easily separated in the recoil energy spectrum. In addition, a series of films made from DM and dDM mixtures were studied. The H and D atom counts per square centimeter were determined directly from the raw data by simulations based on simple models of the film structure. The simplest consisted of a flat slab of uniform composition and variable thickness. A 10.0 nm thick polystyrene film, spin coated on gold from solution (0.3 wt % in chlorobenzene; MW of 10 300, Pressure Chemical, Pittsburgh) to form a uniform planar film, was used as the calibration standard. The surface concentrations were then converted to thicknesses by using a film density of 0.92 g cm^{-3}. Figure 6 shows the resulting thicknesses for a series of PM, dPM, and mixed PM/dPM films plotted against the ellipsometric thicknesses which were determined from the simple fully dense slab model.[51] The correlation shows a least-squares slope of 1.28, quite close to the adjoining

Figure 6. PM film thicknesses determined from QCM (●) and FRES (■) measurements plotted against the ellipsometric thicknesses for the same films. The ellipsometric thicknesses were calculated from the experimental data by using a fully dense PM film model (see above figure). The least-squares slopes of the QCM and FRES lines are 1.34 and 1.28, respectively. Also shown for reference is a line with unity slope. For details see text.

QCM correlation line with a slope of 1.34. This observation shows that the QCM and FRES average film coverages are in excellent agreement and reinforces our earlier conclusions that low ellipsometric thicknesses result from failure to account for the discontinuous nature of the PM films.[49]

8. Chemical Functionalization of Open Film Areas. The evidence that the polymethylene films are characterized by areas of bare gold leads to the possibility that it may be possible to modify the existing gold surface with chemical treatment. One of the most widespread means of doing so is by using long-chain alkane thiols.[52−54] The compound SH−(CH₂)₁₅CO₂CH₃ was used since the presence of the ester group provides a convenient characteristic IRS signature. PM/Au samples with two different film coverages were prepared, immediately characterized by ellipsometry and IRS, and then quickly immersed for 24 h in 0.002 M thiol solutions in ethanol. After removal, the films were thoroughly rinsed in solvent, blown dry in a purified N₂ stream, and characterized again. For comparison, a bare gold surface was exposed to the thiol solution and characterized.

Ellipsometry shows that alkanethiol immersion results in thickness increases which vary inversely with the initial PM coverage. For example, a nominally 0.30-nm PM film showed an increase of 1.8 (±0.1) nm in thickness while a nominally 4.0-nm PM film showed a comparatively smaller increase of 1.5 nm. These data show that open areas exist for the alkanethiol chemisorption and that the thicker film appears to have a smaller fraction of available surface for the thiol.

The IRS data confirm the chemisorption of thiol. The low-frequency region, which provides the most detailed comparison, is shown in Figure 7 for the example of the 4-nm film. The spectra not only reveal the presence of new features associated with the incorporation of thiol molecules and but also show little perturbation of the initial PM spectral features. This observation demonstrates that the thiol has not displaced any significant amount of PM from the gold surface. In fact, the

---

(51) More sophisticated film models in which corrections were made for variable recoil trajectories from the nanometer-sized PM clusters did not result in appreciable changes in the calculated thicknesses. On average, the recoiling ions will traverse through various regions of dense PM, gold (especially in the thinner films where clusters can nucleate in depressed gold defects), and void regions. Since the stopping power of each of these regions differs significantly there will be a skewing of the energy-yield spectrum as a function of the actual film morphology. In general, in view of the low-energy resolution of the detector, equivalent to ~60−80 nm depth resolution, significant errors do not arise from variable morphologies in PM films of less than 30−40 nm thicknesses. The effect of variable void fraction was simulated by assuming the recoil spectrum to be composed of contributions from isolated microscopic slabs of differing thicknesses. Simulations performed with use of the RUMP package showed almost negligible changes in total energy spread at the detector for a variety of slab morphologies, and the recoil ion yields essentially remain linear with the average film thicknesses.
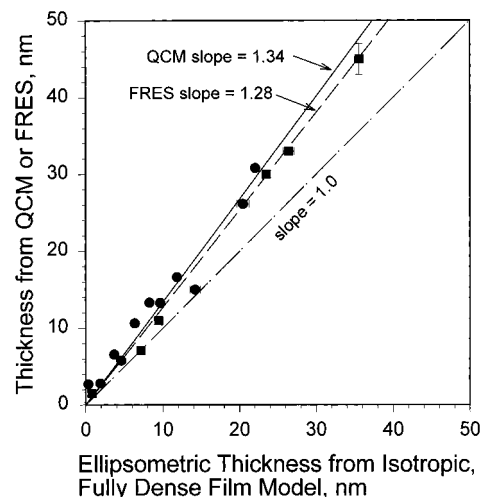
(52) Porter, M. D.; Bright, T. B.; Allara, D. L.; Chidsey, C. E. D. *J. Am. Chem. Soc.* **1987**, *109*, 3559−3568.
(53) Nuzzo, R. G.; Zegarski, B. R.; Dubois, L. H. *J. Am. Chem. Soc.* **1987**, *109*, 733−740.
(54) Bain, C. D.; Troughton, E. B.; Tao, Y.-T.; Evall, J.; Whitesides, G. M.; Nuzzo, R. G. *J. Am. Chem. Soc.* **1989**, *111*, 321−335.
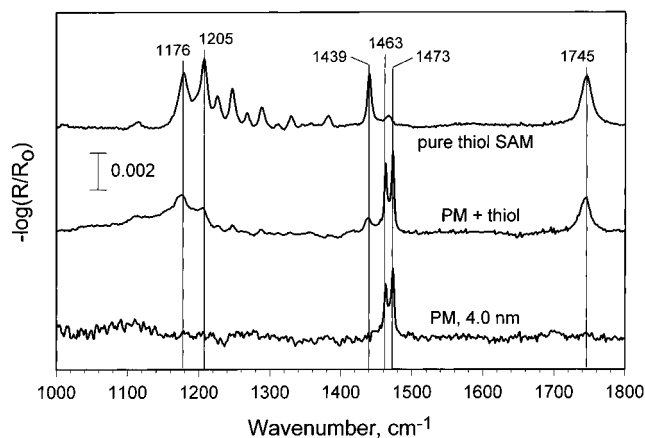
Figure 7. Infrared spectra of a 4.0-nm PM film before and after immersion in a $HS(CH_2)_{15}CO_2CH_3$ solution in ethanol. The top and bottom plots are shown for reference and represent the spectra of a fully formed self-assembled monolayer of the thiol on an initially bare gold surface and of the initial 4.0-nm PM film before thiol solution immersion, respectively.

Figure 8. C−H stretching mode infrared spectra of 4.0- and 44.0-nm PM films heated and cooled to various temperatures. Spectra were obtained directly from the heated samples. The films were held at 136 °C for 45 min before cooling.

two-component spectrum actually shows a slight (∼20%) increase in the PM CH_2 deformation intensity, an effect probably arising from spectral (electromagnetic) perturbations caused by the presence of an adjacent alkanethiolate phase. The top two spectra in Figure 7 show that the organization of the ester thiolate in the PM sample is not as high as is observed in the pure SAM, particularly shown by the decrease in resolution and intensity of the twist−wag progression bands between 1150 and 1350 cm^{-1}, an observation that signifies the appearance of *gauche* defects in the chains. This suggests that the open surface areas may not be continuous enough to support large correlation lengths of ordered SAM because of adsorbed contaminant molecules and/or the presence of a few isolated PM chains. One can note that the general line shape and frequency of the C═O stretching mode at 1745 cm^{-1} is essentially unchanged, but the intensity is diminished by ∼$^1/_3$ in the two component film. This drop could occur for various reasons, including reorientation of the C═O bond and/or electromagnetic medium effects (see above). If these other effects are ignored one can interpret the drop in terms of a simple loss of ∼$^1/_3$ of the open gold surface due to occupation by PM clusters. Applying this interpretation to the data from the 0.30-nm films results in an estimated drop of <20% in the total gold surface area caused by the presence of the PM clusters. Independent electrochemistry experiments corroborate these open area estimates within ∼±10% in the coverages.[55]

9. Thermal Behavior. A series of PM/Au films under N_2 were exposed to various temperatures and the IRS spectra monitored directly at each temperature. Film disordering was observed near 135 °C, corresponding to the reported melting point of bulk polyethylene.[56] The experimental protocol involved heating freshly prepared films to 136.5 °C, conditions which cause chain melting, holding at this temperature for 45 min, and finally cooling back to ambient at a rate of 0.5 deg/min.

As a prelude, we note that the annealing behavior depends significantly on the film coverages, as will be detailed below. A general observation is that the overall topography of the films did not change much with annealing. Of specific interest, AFM images of low-thickness films with patchy coverages did not
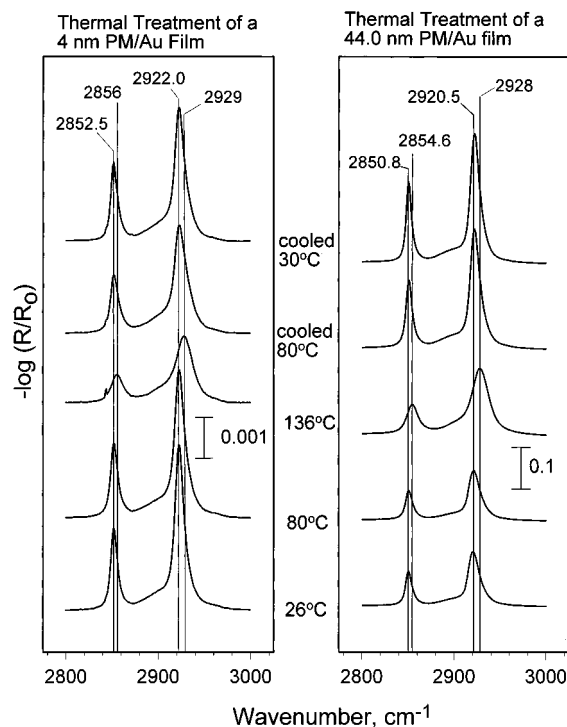
point toward any significant changes in the overall cluster size after annealing, e.g., a spreading out across the surface ("wetting"). This result indicates that the polymer is strongly attached at the nucleating Au defect site and the surface tension of the hot cluster is sufficiently high to overcome any tendency for spreading.

For a closer look at the molecular details of the annealing process, Figure 8 shows that when both the 4.0- and 44.0-nm films are heated to 136 °C the C−H stretching intensities decrease, the line widths broaden, and the peak frequencies shift to higher values, all well-established signs of chain melting. One general feature to note is that for all film thicknesses the stretching frequencies after annealing (Figure 8) do not reach the limit for a completely dense packed, all-*trans* chain phase, values several cm^{-1} below the observed frequencies (see Section 4.4.a). This observation establishes that residual conformational disorder remains after thermal cycling. This state could arise, at least in part, from the presence of amorphous surface layers, primarily chain folding regions, which may be intrinsically associated with the high surface/volume ratio crystals, as observed for polyethylene single crystals.[57]

We focus first on the behavior of the 44-nm film. The line-width changes, which are very sensitive to chain disordering, are summarized in Figure 9. These data show that the onset of calamitous chain disordering occurs at ∼125 °C and substantial hysteresis arises upon cooling. While the d$^+$ and d$^-$ peak frequency changes are almost exactly reversible, irreversible effects are clear in the line widths and intensities. The peak frequency behavior indicates that upon cooling chain recrystallization occurs, but the line width decreases show that the crystalline character is enhanced in the annealed film. The interpretation of the significant intensity increase upon cooling is more complex. Given that the total film mass remains constant with thermal cycling, only film morphology and chain

(55) Seshadri, K.; Allara, D. L.; Guiseppi-Elie, A. Manuscript in preparation.
(56) Mandelkern, L.; Hellman, M.; Brown, D. W.; Roberts, D. E.; Quinn, F. A., Jr. *J. Am. Chem. Soc.* **1953**, *75*, 4093.
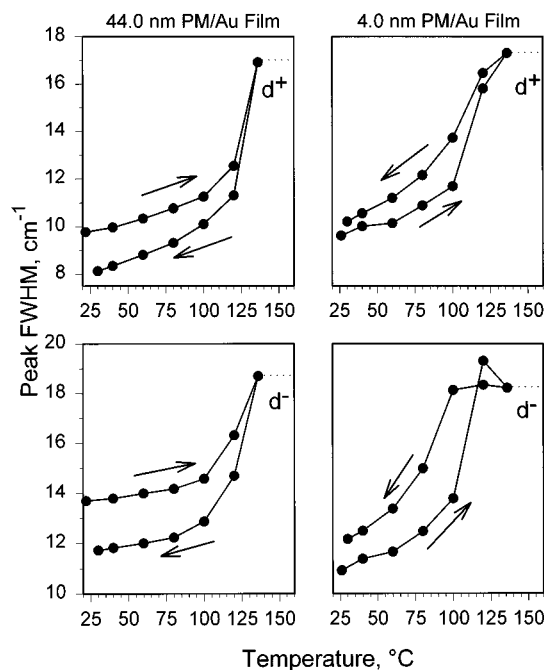(57) Peterlin, A.; Zachmann, H. G. *J. Polym. Sci., Part C* **1971**, *34*, 11−17.

Figure 9. C−H stretching mode line widths (fwhm = full widths at half maximum) as a function of temperature for sample cycled between room temperature and 136 °C. The dotted lines at the top of the curves signify that above the upper temperature no significant changes in fwhm values are observed with further temperature increases within a small range. The heating and cooling legs on the curves are shown by arrows. Note that the thin film shows an inverted behavior relative to the thick film in terms of the change in the fwhm values on heating and cooling. The large broadening of the fwhm values at the upper temperatures signifies conformational disordering of the chains while the return to the lower values upon cooling signifies a return of conformational ordering.

orientation effects could be responsible for this increase. First, changes in the film morphology, *viz.*, clustering and void content, could give rise to increases in the local electric fields via screening effects which would increase the excitation of the oscillators.[58] However, this effect can be discounted from the AFM, ellipsometry, and wetting data (see above) which show no significant changes in cluster geometries with annealing. Second, chain reorientation could affect the intensities by realignment of the transition dipoles of the d⁺ and d⁻ modes more parallel to the surface normal, the direction of the surface electric field which is responsible for exciting the vibrations.[27,47] This seems to be the correct explanation. One can notice that the d⁺ to d⁻ intensity ratios remain constant before and after heating. This is consistent with a constant orthorhombic packing in which the chain planes are set at ∼90° and is confirmed by the constant appearance of doublets for the rocking and scissoring CH₂ modes in the low-frequency spectra (see below). Since this chain configuration establishes a uniform d⁺ to d⁻ intensity ratio at all tilt angles of the crystallites,[27,58] and since the d⁺ and d⁻ transition moments are perpendicular to the chain axis, it follows that the overall intensity increase after thermal cycling must result from realignment of the chain axes toward parallel with the gold surface.

The general annealing behavior of the 4.0-nm film is similar to that of the 40-nm film, in that chain disordering occurs near 136 °C and crystallinity returns upon cooling, but there are significant differences in detail. First, the onset of the disordering process as indicated by the line-width changes (Figure 9) is less sharp than for the thick films, which indicates a smearing
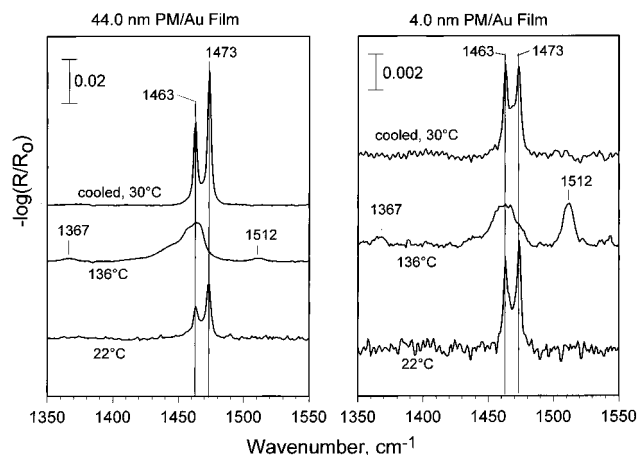
(58) Tao, Y.-T.; Hietpas, G. D.; Allara, D. L. *J. Am. Chem. Soc.* **1996**, *118*, 6724−6735.

Figure 10. CH₂ bending mode spectral changes as functions of temperature for 4.0- and 44.0-nm PM films. The collapse of the doublet structure at the upper temperature signifies the loss of crystalline order while its return on cooling shows recrystallization. Note the appearance of the peaks at 1367 and 1512 cm⁻¹ in the 136 °C spectrum. Both peaks reversibly appear and disappear with thermal cycling and thus are intrinsic to the sample. The former could be a CH₃ feature while the latter is unassigned.
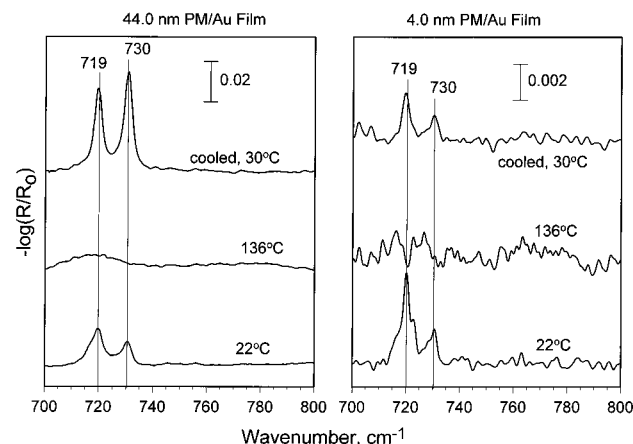

Figure 11. CH₂ rocking mode spectral changes as functions of temperature for 4.0- and 44.0-nm PM films. The collapse of the doublet structure at the upper temperature signifies the loss of crystalline order while its return on cooling shows recrystallization.

of the disordering transition with decreasing film thickness. Second, completely opposite to the behavior of the 44-nm film, upon cooling back to ambient temperature, the intensities of the 4 nm film spectrum, relative to the initial ambient state, show a slight *decrease* while the d⁻ line width actually returns to a slightly *higher* value than the original one. Third, there is relatively little change in intensities upon cooling, which according to the explanation for intensity changes in the 44-nm film (see above) means that there is little chain reorientation. We believe that all these observations signify that a higher degree of chain conformational constraint exists in the ultrathin films due to the highly localized nature of the clusters. In this picture, the clusters are pinned in constrained, nonequilibrium configurations at and within defect and grain boundary regions in the gold surface with sufficiently large Au-cluster interaction energies (van der Waals) such that even at the elevated temperatures large-scale segmental reorganization of the PM chains is quite slow relative to that of the majority of the chains in the thick film structures.

The corresponding low-frequency region data are given in Figures 10 and 11, and examination of the detailed features shows a behavior in agreement with that derived from the C−H

stretching spectra. Again we focus on the behavior of the thicker film first. The spectra show the expected collapse of both the CH_2 scissors deformation and the rocking mode doublets (see Section 4.4.2) at the upper temperature, where the C−H stretching mode spectra (Figure 9) also show chain disordering, and show their reappearance upon cooling, an indication of the restoration of the crystalline packing. However, there are significant hysteresis effects. In the case of the scissors deformation (Figure 10), the cooled film exhibits narrower and more intense lines, relative to the original ambient spectrum, which indicates that the annealed film exhibits improved chain packing, as well as reorientation of the chain axes more toward parallel with the surface. The latter interpretation follows directly from the discussion above for the interpretation of the C−H stretching peak intensity changes since the C−H stretching and CH_2 bending modes have the same transition dipole directions. The rocking mode band shows a similar trend upon cooling of an increase in the doublet resolution and intensity. This confirms the increased crystallinity with annealing. Analysis of the integrated intensities of the rocking peaks for spectra of films in the 20−44 nm thickness range (data other than the 44 nm film not shown) shows that the orthorhombic crystalline content increases from ∼60−65% before annealing to ∼91−96% after annealing (see section 4.4.b).

The 4-nm film shows the same overall disordering behavior as the 44-nm film in that upon heating to the upper temperature both low-frequency modes show a doublet collapse. However, the cooling behavior is significantly different than with the thick film case. Upon cooling the disordered 4-nm film to ambient temperature, the doublets return to their near-original state, save for a slight lowering in the 1473 cm^{-1} scissors peak intensity but a near-halving of the 720 cm^{-1} rocking mode one. While the restoration of the doublets clearly indicates a return to crystalline-containing structure upon cooling, the rather strong changes in the rocking mode doublet intensity ratio indicate that some aspects of the film morphology have changed significantly. Qualitatively, the decreased intensity ratio I_{730}/I_{720} suggests that some improvement in crystallinity has occurred, but to a significantly lower extent than for the 44 nm film case.

In addition to the appearance of the expected rocking and scissors deformation modes in the low-frequency spectra in Figures 10 and 11, we also note the presence of other features at ∼1387 and 1512 cm^{-1} in the scissors mode region in Figure 10. The 1387-cm^{-1} peak could be due to the presence of CH_3 groups for which the symmetrical bending (umbrella) mode typically appears near this position in alkanes. The appearance of this peak, which is very weak in the case of the 44-nm film but a bit stronger in the 4.0 nm film case, is consistent with the observation of a CH_3 characteristic stretching band in Figure 4 for a 1.0-nm film and supports the existence of a radical disproportionation chain termination (reaction 3) for the PM polymerization.[59] More unexpected is the feature at 1512 cm^{-1}, which appears with significant intensity in the 4 nm film spectrum (Figure 10). The source of this band is puzzling since no typical mode of a polymethylene chain should arise near this frequency. However, the strong correlation of its appearance with heating and cooling shows that it is related to an intrinsic property of the PM films. Since its presence is heightened in the ultrathin film we speculate that it is associated

with a feature of chains with highly constrained structures pinned at gold surface defect sites.

10. Deliberately Roughened Substrates. Since the above data indicated that the morphology of the gold surface plays an important role in the formation of the clusters, a brief investigation of the effects of surface roughness was carried out. Deliberately roughened gold substrates, with root-mean-square roughness ∼2−3 times the typical smooth substrates (determined by ellipsometry and AFM), were prepared by performing the depositions at higher pressures.

Ellipsometric measurements indicated the limiting coverages of these rough substrate PM films, prepared by long deposition times in the DM solution, generally reached greater coverages than on smooth substrates (latter data in Figure 1), with limiting equivalent thicknesses as high as ∼80−90 nm observed. The thinner films on the rough substrates show similar water contact angle values as those on smooth substrates. However, for the thicker rough films in the range of ∼25−60 nm, the contact angles are higher than similar thickness smooth films, with values reaching as high as 140° for the highest coverage rough films in comparison to the limiting values of ∼103° for the smooth ones (Figure 2). These extraordinarily high values are also accompanied by a very large hysteresis of ∼60°, as compared to ∼30° for the thinner (≲20 nm) rough substrate films. These data indicate that the high-coverage rough substrate films are characterized by a very rough wetting surface topography that provides non-uniform contact lines and presents a wetting contact area significantly greater than the geometric area. At these high PM coverages one can assume that the wetting surface consists purely of PM so Young's equation can be modified to account for the roughness through introduction of a roughness coefficient:[60]

$$\cos(\theta_r) = r \cos(\theta) \tag{5}$$

where θ is the contact angle on a flat surface of the component, θ_r is the measured contact angle on the rough surface, r is the roughness factor, which is most simply the ratio of the actual area presented by the surface to the projected area[61] and can be related to the fractal dimension of the surface, and the constraint $r \cos(\theta) \leq 1$ applies. The equation predicts an increasing contact angle with roughness for $\theta > 90$. Using this equation, we estimate that a 140° contact angle results from $r \sim 3.8$. These results are very similar to recently reported work on highly rough alkylketene dimer surfaces.[62] In our case, the increasing roughness can be due to a convolution of the intrinsic Au roughness and any increased nucleation of PM clusters which will cause a rougher PM morphology.

The IRS spectra of the rough substrate films are similar to those seen for the smooth substrate cases. However, the spectra of ∼ 60-nm films do show the presence of $CH=CH_2$ groups indicated by the appearance of peaks at 909 and 1640 cm^{-1}, typical of the vinylic C−H bending C=C stretching frequencies, respectively. According to the mechanism suggested earlier in reaction 3, these data indicate that some chains possess vinyl groups at the chain termini and thus the average sequence length is shorter on the roughened surfaces than on the smooth surfaces.

Annealing of films is accompanied by a reduction in ellipsometric thickness, as well as distinct morphological changes. The ellipsometric thickness decrease ranges from a few percent for thinner films to as much as 30% for the thickest

(59) However, we note that the appearance of this mode is somewhat inconsistent from sample to sample and that its tendency to appear in the thinnest film spectra indicates that the presence of the CH_3 group seems enhanced for chain polymerization near the gold surface. Given that the CH_3 group appears as a result of chain termination via reaction 3, these observations imply that the degree of polymerization may be lower near the Au/PM interface.

(60) Adamson, A. W. *Physical Chemistry of Surfaces*, 5th ed; John Wiley & Sons: New York, 1990; Chapter X, Section 4.

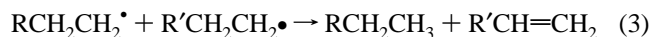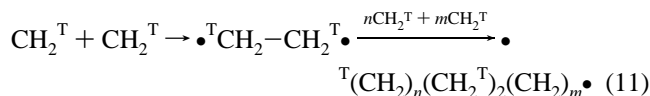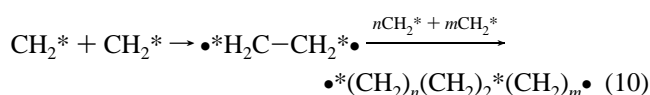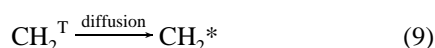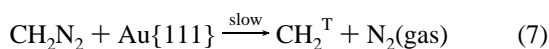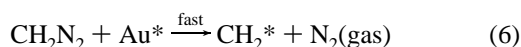(61) Hazlett, R. D. *J. Colloid Interface Sci.* **1990**, *137*, 527.

(62) Onda, T.; Shibuichi, S.; Satoh, N.; Tsujii, K. *Langmuir* **1996**, *12*, 2125−27.

films. Since no material is lost, the change in ellipsometry parameters signifies a change in the morphology. For the 60-nm film, annealing results in a foggy surface, indicating a recrystallization of the polymer chains into larger clusters that scatter the light. The water contact angles remain unchanged (±2°) for films ≲30 nm. However, in the case of the thicker films, which exhibit abnormally high contact angles (∼130−140°), annealing results in a lowering of the contact angle to around 110°, together with a diminished hysteresis (∼40°). This is difficult to interpret in terms of the surface morphology, but could mean that there is a reorganization of the chains that results in a lower value of *r*. A general observation for the IR spectra is that the C−H stretching intensities increase upon annealing, similar to the observation with smooth substrate films. However, the vinylic peak at 909 cm⁻¹ persists and increases in intensity while the C=C stretch peak nearly vanishes. This may also suggest a reorientation of the mostly *all-trans* zigzag molecular chains, from a partially perpendicular orientation to the gold surface (local surface, not the geometric) to a more parallel one.

5. Discussion

1. Overall Observations. Our results show that diazomethane decomposes on relatively smooth, polycrystalline Au-{111} surfaces to yield crystalline polymethylene. In the early growth stages the polymer appears as nanometer-size clusters localized in substrate grain boundary and defect regions, but as thicknesses approach the ∼20−40-nm scale the clusters eventually coalesce to form a uniform substrate coating. The polymer exhibits conformationally ordered chains packed in an orthorhombic arrangement, but significant *gauche* defects exist, especially in the thinnest films, relative to other forms of crystalline PM chains such as exist in *n*-alkanes. The observation of a significantly enhanced thermal annealing of the crystallites in the thicker films suggests that in the early growth stage, the isolated clusters are pinned at gold defect sites with surface constrained chains which cannot fully anneal to highly ordered phases. The observation that the regions between the clusters are accessible to chemisorption by alkanethiol molecules shows that the PM chains do not extend significantly into the intercluster regions in these low-coverage films and that the PM clusters are tightly bound and conformal to the gold surface such that displacement by thiol groups does not occur to any significant extent under our chemisorption conditions.

2. The Polymerization Mechanism. The data reveal evidence for the polymerization mechanism and likely steps are indicated in reactions 6−12. Reaction 3, the termination step mentioned earlier, has been shown again for convenient reference. In the equations, *, T, and •, respectively, designate a Au surface defect site location, a Au{111} terrace location, and a C-radical. Each of these steps is discussed in terms of the experimental evidence.

$$CH_2N_2 + Au^* \xrightarrow{fast} CH_2^* + N_2(gas) \quad (6)$$

$$CH_2N_2 + Au\{111\} \xrightarrow{slow} CH_2^T + N_2(gas) \quad (7)$$

$$CH_2^*(\text{site a}) \xrightarrow{diffusion} CH_2^*(\text{site b}) \quad (8)$$

$$CH_2^T \xrightarrow{diffusion} CH_2^* \quad (9)$$

$$CH_2^* + CH_2^* \rightarrow \bullet^*H_2C{-}CH_2^*\bullet \xrightarrow{nCH_2^* + mCH_2^*}$$
$$\bullet^*(CH_2)_n(CH_2)_2^*(CH_2)_m\bullet \quad (10)$$

$$CH_2^T + CH_2^T \rightarrow \bullet^TCH_2{-}CH_2^T\bullet \xrightarrow{nCH_2^T + mCH_2^T} \bullet$$
$$^T(CH_2)_n(CH_2^T)_2(CH_2)_m\bullet \quad (11)$$

$$CH_2N_2 + \bullet(CH_2)_nR \rightarrow \bullet(CH_2)_{n+1}R + N_2(gas) \quad (12)$$

$$RCH_2CH_2^\bullet + R'CH_2CH_2\bullet \rightarrow RCH_2CH_3 + R'CH{=}CH_2 \quad (3)$$

a. Polymerization Is Initiated at Gold Defect Sites. The first important observation to consider is that at low film coverages the clusters are localized in gold surface defect sites. This observation shows that the polymerization is defect initiated, forcing chain propagation to ensue in these localized regions.

The relative enhancement of defect- over terrace-site initiation (reactions 6 and 7, respectively) can be expected since surface Au atoms located in grain boundary defect regions have lower lattice coordination numbers and higher energies than those in dense {111} terraces. For example, it is known that mechanical scratching produces high-energy surface defects that are favorable for the adsorption of olefins and other hydrocarbon species.[63] Estimation of the surface energy for different Au surface orientations has been made from measurement of the zero-charge potentials,[64] and the observed trends indicate that the highest energies are found for the high-index planes around the (111) point in the stereographic triangle [planes such as (554), (332), etc.], the typical planes expected in the grain boundary regions of a {111} textured surface. Self-diffusion data for Au in the lattice and grain boundaries have been used to give an estimate of 390 erg/cm² for the average excess surface energy of an atom in the grain boundary region.[65] Although Au surfaces, relative to other coinage metals such as Cu,[66,67] are not typically considered as supporting strong coordination with carbon radical species, some degree of coordination with CH₂ can be expected at the high energy defect Au* sites to form H₂C=Au* species, designated in the equations as CH₂*. The coordination from these high-energy sites can be expected to provide enough stabilization to lower the ∼7 kcal/mol[68] nitrogen extrusion barrier height for carbene formation and make reaction 6 quite fast relative to reaction 7.

Two chain propagation routes for the CH₂* species are possible: diffusive addition of adjacent CH₂* species (reaction 8 + reaction 10, a Langmuir−Hinshelwood process) and addition of DM (reaction 12, cast as, but not necessarily, an Eley−Rideal process). In the absence of side reactions, e.g., oxidation by adventitious impurities and O₂, and given the relatively weak bonding to Au (e.g., compared to active transition metals such as Ni), the CH₂* species will be available in significant concentrations in the immediate vicinity of the defect region where they are generated and should be highly reactive.

The primary propagation step in reaction 10 forms the •*H₂C−CH₂*• species which then can propagate at both ends via CH₂* addition to form polymeric biradical RCH₂*• units,[69]

(63) Mori, S.; Shitara, Y. *Appl. Surf. Sci.* **1993**, *68*, 605−7.

(64) Hamelin, A.; Lecoeur, J. *Surf. Sci.* **1976**, *57*, 771−4.

(65) Gupta, D. *Philos. Mag.* **1976**, *33*, 189−97.

(66) For example, see: Bent, B. E. *Chem. Rev.* **1996**, *96*, 1361−1390.

(67) There is specific precedent for these species involving a coinage metal atom. For example, reactions of Cu atoms with diazomethane in Ar matrices at low temperatures [Chang, S.-C.; Kafafi, Z. H.; Hauge, R. H.; Billups, W. E.; Margrave, J. L. *J. Am. Chem. Soc.* **1987**, *109*, 4508−13. Chang, S.-C.; Hauge, R. H.; Kafafi, Z. H.; Margrave, J. L.; Billups, W. E. *Inorg. Chem.* **1990**, *29*, 4373−6] are reported to spontaneously form the primary insertion products Cu=CH₂ and N₂Cu=CH₂, as well as the adducts Cu(CH₂N₂).

(68) Yamamoto, N.; Bernardi, F.; Bottoni, A.; Olivucci, M.; Robb, M. A.; Wilsey, S. *J. Am. Chem. Soc.* **1994**, *116*, 2064−74.
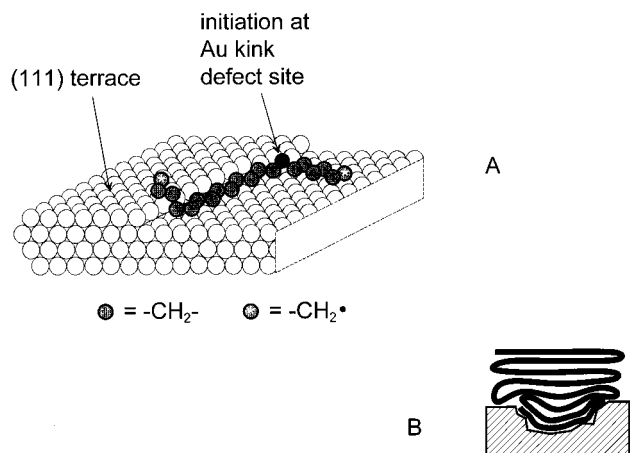
Figure 12. (A) A cartoon schematic of a $-(CH_2)_x-$ chain initiated at and growing from a kink defect site along a step between two Au-(111) terraces. The picture conveys possible features of the proposed polymerization mechanism at substrate defect regions as given in the text. The picture shows growth of linear $-(CH_2)_x-$ in one direction out onto the adjacent terrace and in the other direction along the step edge and up over the step riser onto the elevated terrace. (B) A cartoon representation of the proposed vertical gradient in chain order for PM clusters initiated at a gold pit type of defect. The initial growth involves the chain vector propagation conformal to the disordered substrate surface, but at later growth stages where stacks of lamellae are formed the memory of the substrate disordered diminishes and the chains become more highly ordered. The tight binding of the bottom layer of disordered chains to the gold substrate constrains these chains from increased ordering upon thermal annealing. For details see text.

indicated by the $*$ as remaining coordinated to the gold surface and where R also contains a radical terminus. An idealized schematic of the early stages of PM growth initiated at a Au kink site on a step, typical of the many types of high-energy defects on an evaporated Au surface, is shown in Figure 12A. This figure shows the chain initially growing along the step riser and implies that CH_2* species tend to congregate here. A recent STM study of benzene on Cu(111)[70] shows that at low temperatures a 2-D adsorbate gas tends to collect and diffuse along step edges, similar to the above picture for the Au{111} surface. This implies that some fraction of CH_2^T species also might eventually diffuse to a more energetically favorable adjacent grain boundary region where they subsequently can contribute to the chain propagation, indicated by reaction 9. In the early growth stage pictured in Figure 12A, the chain will be expected to propagate along the substrate surface in order to maximize the van der Waals (dispersive) interactions of the $-(CH_2)-$ chains with the strong attractive potentials of the gold surface atoms, thus forcing the chain vector to conform to the local surface topography which, in the case of gold defect regions, will introduce significant *gauche* defects into the chains. Our observation of a significant resistance of the clusters in thin films to improve their crystalline content under thermal annealing (Section 4.9), in contrast to the effective annealing

of the thick films, is quite consistent with this picture of surface-constrained, defect-populated chains. Although the present signal/noise in the IRS measurements precludes the clear observation of the thermal order−disorder transitions for the thinnest films (<1 nm) with the highest content of constrained chains, we believe that the transitions in these films will be extensively smeared or even destroyed by the chain pinning at the gold surface.

b. The PM Clusters Consist of Layers of Chains. The second important observation is that the clusters grow to thicknesses far in excess of 0.5 nm, the thickness of a single $(CH_2)_x$ chain. This shows that the propagating chain vector (see Figure 12A) must move away from the surface at some point with the polymerization continuing on top of an underlying layer of PM chains. Since it seems unlikely that significant concentrations of CH_2* species will diffuse onto and across a PM surface, resulting in loss of the Au coordination energy, it is expected that propagation in the later stages must occur by direct addition of CH_2N_2, as shown by reaction 12. In order to obtain the observed crystalline morphology, the growing chain vector at the PM surface must follow the surface topography and align with the underlying PM chains. In addition, in order to form the clusters to the observed heights it is necessary for the chains to continue to fold into lamellae. This mechanism provides a limit to an isolated cluster height since once chain termination occurs, no new chain initiation can arise on the cluster surface. However, if a new cluster forms adjacent to a previous one, it is reasonable to expect that the new growth can propagate along the surface of the previous cluster, thus forming overall thicker films. On the basis of this growth model, we speculate that the defect-pinned clusters likely possess a gradient of chain defects in which the chains in the regions of the substrate are significantly conformationally disordered (see above) due to the gold defect topography while the chains at the top surface of the cluster have become more highly ordered as memory of the initial disordered substrate template becomes lost with increasing layering of the lamellae. A picture suggesting the essence of this structure is given in Figure 12B.

c. Later-Stage Growth Occurs on Gold Terraces. The third important observation is that at intermediate coverages, ≥20 nm, the growth begins to spill out onto the {111} terraces. At this point, one can assume that the high-energy Au* sites have been covered and the slower growth on the {111} terraces takes over, shown by reactions 11 and 12. This change is indicated by the roll-off in rates shown in Figure 1. At this point, since all sites on a perfect {111} terrace are identical, one can assume that the initiation ensues uniformly across the surface and that growth accordingly occurs in an approximate 2-D manner.[71] Finally, at sufficiently large coverages, the PM growth completely stops. This must arise because of the complete blocking of the gold surface, thus shutting down the initiation steps 4 and 5.

3. Connections to Transition Metal Surface Catalyzed Hydrocarbon Synthesis. Finally we remark that the above polymerization mechanism represents a very useful limiting case of the reaction chemistry of surface-adsorbed methylidene species. This chemistry is a subject of immense interest because of its relevance to hydrocarbon polymerization processes such as the Fischer−Tropsch (FT) process which involve intermediate alkylidene and carbon radical species to produce short and intermediate chain length hydrocarbons.[66,72] Typical FT catalysts, which utilize such transition metals as Cu and Fe, strongly

(69) There are generalized precedents for this type of chain propagation. For example, in a study of homogeneously-catalyzed DM polymerization by transition metal complexes it was observed that in the case of (cycloocta-1,4-diene)PtCl(CH₃) a Cl ligand is displaced by CH_2 to form Pt=CH₂ and that subsequent CH₃ ligand migration from Pt further forms a PtCH₂CH₃ species [McCrindle, R.; Arsenault, G. J.; Farwaha, R.; Hampden-Smith, M. J.; McAlees, A. J. *J. Chem. Soc., Chem. Commun.* **1986**, 1943]. This mechanism has the underlying requirement that the alkyl group formed should have good migratory flexibility. While this requirement is probably satisfied better in the solution phase as compared to the surfaces in our study, it is clear that PM chain growth on the Au surface could likely occur by transfer of CH_2 units from CH₂=Au species to growing chain ends.

(70) Stranick, S. J.; Kamma, M. M.; Weiss, P. S. *Science* **1994**, *26*, 99−102.

(71) Preliminary high-resolution AFM images of films in the intermediate stages of growth show features on the {111} terraces which appear to be single chains. [Seshadri, K. Allara, D. L. Unpublished results.]

adsorb intermediate C$_x$H$_y$ species, allow facile surface−adsorbate H atom transfer and coupling of intermediates, but minimize C−H and C−C bond cleavage and only weakly bind product hydrocarbons. Gold represents a near-limiting case of a surface with no propensity for C−H bond cleavage and a weak coordination with intermediate C$_x$H$_y$ species.[73] The DM/Au system maximizes coupling reaction efficiency by allowing fast diffusion and reaction[74] of the weakly bound CH$_2$ species, relative to C−H and C−C bond cleavage. In fact, this efficiency is so high that even in the presence of good solvents (e.g., diethyl ether in the present case), formation and desorption of small hydrocarbon products such as C$_2$H$_4$ and short chain −(CH$_2$)$_x$− oligomers cannot occur to a sufficient extent to prevent the formation of polymers. This parallel has been the subject of earlier studies,[75,76] but the present one appears to be the first which definitively characterizes the structure of the polymer that forms and its general relationship to the metal substrate morphology.

6. Conclusions and Future Work

Our results show that linear, crystalline −(CH$_2$)$_x$− polymers form via DM decomposition and CH$_2$ polymerization at gold surfaces. Initial polymerization occurs at substrate defect sites to form nanometer-sized PM clusters. At later stages, growth initiates on the gold terrace regions, and finally all gold sites become blocked stopping the polymerization. The thermal annealing data reveal a very interesting structural picture in which chains formed adjacent to the rough topography gold defect sites are constrained by the strong substrate attractive potential to remain in high *gauche* defect forms while the top layers of the clusters and the terrace films exhibit much higher initial orders with less constrained order−disorder behavior. Experiments to observe the sharpness of the thermal transitions as a function of thickness down to the <1 nm region are underway with high-sensitivity IRS measurements.

The polymerization mechanism provides a limiting case of a highly efficient surface-mediated coupling of CH$_2$ species on a transition metal. Coupling reactions of small hydrocarbon fragments are of great interest in surface-catalyzed hydrocarbon synthesis, and the present work provides some insight on how efficient these processes can be. Along these lines, work is in progress on systematically studying these polymerizations by means of both structural and kinetic measurements with use of different metals, in particular copper; single crystal substrates, including Au, with controlled surface structures; and variations of the starting diazoalkanes, including mixtures and isotopic labeling.

Finally, we note that DM decomposition on Au surfaces provides an effective way to cover substrate defect sites with a tenacious, highly hydrophobic, insulating "filler" that blocks the gold sites from interactions with the outside environment. This allows formation of an interesting new class of chemically heterogeneous surface structures by self-assembly of alkanethiols in the open terrace regions of partial coverage PM/Au films. Formation of a variety of these structures and exploration of their properties, such as electrochemical and wetting responses, is currently in progress.

(72) For a general reference see: Somorjai, G. *Introduction to Surface Chemistry and Catalysis*; John Wiley: New York, 1994; Chapter 7.

(73) In contrast, even on the closely related coinage metal Cu, adsorbed CH$_3$ radicals and CH$_2$ are tenaciously bound on the (110) surface with bond enthalpies of 33 and 75 kcal/mol, respectively [Chiang, C. M.; Wentzlaff, T. H.; Bent, B. E. *J. Phys. Chem.* **1992**, *96*, 1836−1848]. Given the typical comparisons in coordination strengths of ligands between similar Cu and Au complexes, these data suggest that while some coordination between defect Au atoms and CH$_2$ can definitely be expected, it should be considerably lower than that for Cu.

(74) The activation barriers for most CH$_x$ reactions on Cu are near zero [Shustorovich, E. *Catal. Lett.* **1990**, *7*, 107−118]. Since this will hold for Au as well, the rate of reaction 10 will be diffusion limited.

(75) Brady, R. C., Pettit, R. *J. Am. Chem. Soc.* **1981**, *103*, 1287.

(76) Smutek, M. *J. Mol. Catal.* **1984**, *24*, 257−60.